Communications on Applied Nonlinear Analysis
ISSN: 1074-133X
Vol 32 No. 8s (2025)

Slip Effects on Unsteady MHDCASSON Nano Fluid Flow Over a Porous Stretching Sheet

Tanuja Rachakonda[1], G. Venkata Ramana Reddy[2], Boina Anil Kumar[3]
[1,3]Department of BSH (Mathematics) SOS, GIETU, Gunupur-765022.
[2]Department of Mathematics, Koneru Lakshmaiah Education Foundation, Green Fields, Vaddeswaram, Guntur (Dt)-India- 522302.
Email: tanujarachakonda19@gmail.com, anilkumarboina@gmail.com, gvrr1976@gmail.com

Article History:

Received: *29-10-2024*

Revised:*03-12-2024*

Accepted:*30-12-2024*

Abstract:

A rigorous theoretical investigation has been conducted to elucidate the prominent characteristics of slip phenomena on magnetohydrodynamic (MHD) Casson nanofluid flow across a porous stretching sheet, wherein the effects of the Soret effect, thermal radiation, and chemical reaction are analyzed numerically. We consider the magnetic field applied and the time-dependent stretching sheet, which is characterized by a non-uniform velocity profile. For the purpose of transforming the governing partial differential equations into a system of coupled nonlinear ordinary differential equations, appropriate similarity variables are employed. The resulting transformed equations are subsequently resolved numerically utilizing the Runge-Kutta Fehlberg method in conjunction with the shooting technique. A detailed examination reveals how various physical factors influence the flow properties related to velocity, temperature, and concentration patterns, alongside their effects on the skin friction coefficient, Nusselt number, and Sherwood number, which are illustrated through a collection of insightful graphs and tables.

Keywords: MHD; Casson nano fluid; Soret effect; Stretching sheet; Porous medium;

1. Introduction

Fluid dynamics assumes a crucial role in various practical applications within production processes, particularly in the context of stretching surfaces, which encompass both metal and polymer sheets. These applications include the cooling of an infinitely large metal plate within a cooling bath, the analysis of boundary layers associated with material handling conveyors, the aerodynamic extrusion of plastic sheets, and the investigation of boundary layers in liquid films during condensation processes.

Mahanthesh and colleagues [1] carried out research that investigated how chemical reactions and partial slip affect the three-dimensional movement of a nano-fluid in contact with a surface that is being stretched exponentially. Chamkha and his team [2] looked into similarity solutions that involve suction/injection and the ramifications of chemical reactions for unsteady heat and mass transfer resulting from a stretching surface located in a porous medium. The team led by Hayat [3] investigated the influence of slip conditions alongside heat transfer phenomena on the dynamics associated with peristaltic flow. Motsa et al. [4] pursued a successive analysis concerning the linearization of the effects of partial slip, thermal diffusion, and magnetohydrodynamics (MHD) on the steady convective flow induced by a rotating disc. Shateyi et al. [5] examined MHD mixed convection slip flow occurring on a non-linearly vertical stretching sheet in proximity to a stagnation point, incorporating aspects of viscous dissipation. Prasannakumara et al. [6] analyzed the effects of multiple slip conditions and heat radiation on the MHD flow of Jeffery nanofluids, with a focus on heat transfer characteristics. Mabood et al. [7] addressed the phenomenon of melting heat transfer and the implications of second-order slip and radiation effects on stagnation point flow. In a subsequent investigation, Mabood et al. [8] assessed the consequences of multiple slip conditions on the unsteady MHD heat and mass flow. Sharidan and others [9] explored similarity solutions regarding unsteady boundary layer flow and the related heat transfer phenomena emerging from a stretching sheet. Elbashbeshy et al. [10] conducted an analysis of heat transfer

phenomena over an unsteady stretching surface. Grubka et al. [11] turned their attention to the fascinating world of continuous stretching surfaces, distinguished by their temperature variations that are crucial to the intricacies of heat transfer. An exploration by Magyari et al. [12] into the dynamics of heat and mass transfer revealed insights on an exponentially expanding continuous surface, particularly concerning the boundary layer. Nazar and colleagues [13] investigated the characteristics of unsteady flow in the boundary layer close to a stagnation point on a stretching sheet. The findings of Magyari et al. [14] detailed exact solutions related to permeable stretching surfaces for flows with self-similar boundary layers. Additional intriguing investigations pertinent to flow and heat transfer can be referenced in sources [15–27]. Furthermore, the study investigates the effects of thermal slip on unsteady magnetohydrodynamic (MHD) Casson nanofluid flow over a porous stretching sheet. It reveals that variations in magnetic field strength, angle of inclination, and suction intensity significantly influence the fluid's velocity profiles studied by Aruna et al [28]. Additionally, improved porosity and radiation parameters contribute to an increase in fluid temperature. The research highlights the importance of these factors in optimizing thermal management and enhancing the performance of systems utilizing Casson nanofluids in porous media. The study investigates slip effects on unsteady MHD Casson nanofluid flow over a porous stretching sheet, highlighting the influence of thermal slip conditions and temperature jump by Arick et al [29]. It reveals that the presence of slip enhances the velocity fields and reduces the thermal boundary layer, promoting better heat transfer. The results indicate that manipulating the shearing effect magnitude can control the inverted boundary layer appearance, which is crucial for optimizing thermal management in various applications, including heat exchangers. Reddy et al [30] have studied the that slip effects significantly influence the flow characteristics of a magnetohydrodynamic (MHD) Casson fluid over a porous stretching sheet. An increase in the velocity slip factor leads to a reduction in the velocity field, while enhancing thermal and concentration contours. This highlights the importance of slip conditions in modifying the flow behavior and thermal profiles, which is crucial for applications in engineering and environmental contexts where such fluid dynamics are prevalent.

Upon conducting a thorough review of existing literature, the predominant challenges linked to the present configuration pertain to a detailed investigation of the slip phenomena within unsteady magnetohydrodynamic Casson nanofluid flow, alongside the heat and mass transfer mechanisms influenced by thermal radiation and chemical reactions in the framework of a permeable stretching surface. The importance of physical interpretations concerning the various parameters is elucidated through the employment of graphical representations and systematically organized data sets.

2. Mathematical Formulation

A 2-D unsteady MHD flow of an incompressible electrically conducting Casson nanofluid over a permeable stretching sheet in the presence of thermal radiation and chemical reaction are considered. A coordinate system is chosen in such a way that x-axis is measured along the stretching sheet and y-axis normal to it. Also, it is assumed that the flow takes place for y>0. The sheet is stretched with nonuniform velocity $u(x,t)=\frac{bx}{1-\zeta t}$ along x-axis where b is the stretching rate and ζ is the positive constant with the property $\zeta t<1$. A uniform magnetic field of strength $B(x)=B_0x^{-1/2}$ with $B_0\neq 0$ is applied normal to the sheet and it is assumed that the induced magnetic field is negligible. The temperature and concentration are maintained at prescribed constant values T_w, C_w at the surface and T_∞, C_∞ are the fixed values far away from the surface. Also, it is assumed that the first order homogeneous chemical reaction of species with reaction rate is constant. The flow configuration is shown in Figure 1.

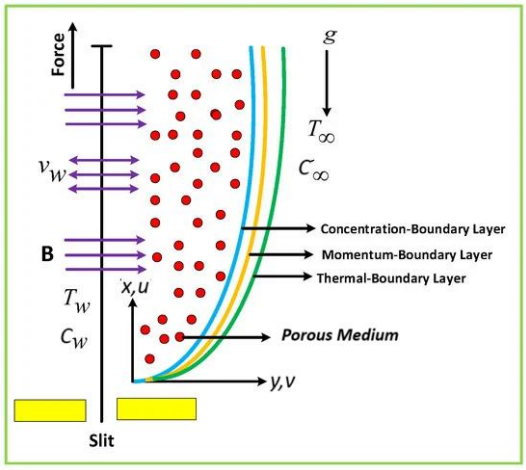

The rheological equation of state for an isotropic and incompressible flow of Casson fluid is given by:

$$\tau_{ij} = \begin{cases} 2\left(\dfrac{\mu_B + P_{y'}}{\sqrt{2\pi}}\right)e_{ij}, & \pi > \pi_{c,} \\ 2\left(\dfrac{\mu_B + P_{y'}}{\sqrt{2\pi_c}}\right)e_{ij}, & \pi < \pi_{c,} \end{cases} \tag{1}$$

where $\pi = e_{ij}e_{ij}$ and e_{ij} represents the component of $(\mathrm{i},\mathrm{j})^{th}$ distortion rate, π being the resulted from distortion rate itself, the product π_c is a critical value reliant over non-Newtonian form, μ_B represents the non-Newtonian fluid viscosity relevant to a fluid of plastic dynamic and P_y gives the fluid yield pressure.

The governing conservation equations under the boundary layer approximation, are as follows:

$$\frac{\partial u}{\partial x} + \frac{\partial v}{\partial y} = 0 \tag{2}$$

$$\frac{\partial u}{\partial t} + u\frac{\partial u}{\partial x} + v\frac{\partial u}{\partial y} - \frac{\sigma B_0^2(x)}{\rho}(u) - \frac{\nu}{K^*}u - \nu\left(1+\frac{1}{\beta}\right)\frac{\partial^2 u}{\partial y^2} = g\beta_T\left(T - T_\infty\right) + g\beta_C\left(C - C_\infty\right) \tag{3}$$

$$\frac{\partial T}{\partial t} + u\frac{\partial T}{\partial x} + v\frac{\partial T}{\partial y} = \frac{\kappa}{\rho Cp}\frac{\partial^2 T}{\partial y^2} - \frac{1}{\rho Cp}\frac{\partial q_r}{\partial y} \tag{4}$$

$$\frac{\partial C}{\partial t} + u\frac{\partial C}{\partial x} + v\frac{\partial C}{\partial y} = D_B\frac{\partial^2 C}{\partial y^2} + \frac{D_T}{T'_\infty}\frac{\partial^2 T}{\partial y^2} - Kr(C - C_\infty) \tag{5}$$

where t denotes the temporal parameter, u and v represent the velocity components along the x and y axes, respectively, ρ signifies the mass density of the fluid medium, n indicates the viscosity coefficient, K$*$ refers to the permeability constant, k denotes the thermal conductivity parameter, D represents the molecular diffusivity, and Kr indicates the rate of the chemical reaction. βT is identified as the volumetric thermal expansion coefficient, βC is characterized as the volumetric expansion coefficient attributable to chemical species, T represents the temperature associated with the species, C signifies the concentration of the species, $T\infty$ and $C\infty$ denote the ambient temperature and concentration, respectively, σ represents the electrical conductivity of the medium, B_0 indicates the magnitude of the external magnetic field, g signifies the acceleration due to gravitational forces, and qr denotes the radiation heat flux emanating from the stretching surface.

The relevant boundary conditions are given in (6):

$$u = u(x,t) + u_{\text{slip}}, v = v_w, T = T_w(x,t) + \mathrm{T}_{\text{slip}}, C = C_w(x,t) + C_{\text{slip}} \text{ at } y = 0$$
$$u \to 0, T \to T_\infty, C \to C_\infty \text{ as } y \to \infty \tag{6}$$

where $v_w = v_0 / \sqrt{x}$ is the suction /injection velocity.

The temperature of the stretching sheet $T_w(x,\mathrm{t})$ and the concentration $C_w(x,t)$ at the surface are assumed as if the following form:

$$T_w(x,t) = T_\infty + T_0\left(\frac{bx}{2\nu}\right)(1-\zeta t)^{-2}, C_w(x,t) = C_\infty + C_0\left(\frac{bx}{2\nu}\right)(1-\zeta t)^{-2} \tag{7}$$

where T_0 and C_0 are the reference temperature and reference concentration are respectively, the above quantities are valid if $(1-\zeta t) > 0$ also $0 \le T_0 \le T_w$ and $0 \le C_0 \le C_w$. In the absence of buoyancy force $b = 0$, which corresponds to the limit of forced convection.

The radiation heat flux (q_r) is modeled by using Rosseland approximation given in (8);

$$q_r = -\left(\frac{4\sigma^*}{3k_1}\right)\frac{\partial T^4}{\partial y} \tag{8}$$

Here σ^* represents the constant of Stefan-Boltzmann, k_1 gives the coefficient of mean absorption. It is also assumed that if the difference in temperature within the flow is T^4, then T^4 can be expressed as a linear combination of the temperature by expanding the T^4 by Taylor's series about T_∞ to obtain (9):

$$T^4 = T_\infty^4 + 4T_\infty^3(T - T_\infty) + 6T_\infty^2(T - T_\infty)^2 + \cdots \tag{9}$$

If we neglect the higher order beyond the first degree in $(T - T_\infty)$ in this series and opening brackets on the righthand sides of (9) we obtain (10):

$$T^4 \approx -3T_\infty^4 + 4T_\infty^3 T \tag{10}$$

Substituting the right-hand side of (10) into (8) for T^4 yield (11):

$$q_r = -\left(\frac{4\sigma^*}{3k_1}\right)\frac{\partial T^4}{\partial y} = -\left(\frac{4\sigma^*}{3k_1}\right)\frac{\partial}{\partial y}\left(-3T_\infty^4 + 4T_\infty^3 T\right) = -\left(\frac{16T_\infty^3\sigma^*}{3k_1}\right)\frac{\partial T}{\partial y} \tag{11}$$

The rate of change in radiative heat flux with respect y is given by (12):

$$\frac{\partial q_r}{\partial y} = -\left(\frac{16T_\infty^3\sigma^*}{3k_1}\right)\frac{\partial^2 T}{\partial y^2} \tag{12}$$

Substitution of (12) into the second term on the right-hand side of (4) changes (4) into (13):

$$\frac{\partial T}{\partial t} + u\frac{\partial T}{\partial x} + v\frac{\partial T}{\partial y} = \alpha\left(1 + \frac{16T_\infty^3\sigma^*}{3k_1}\right)\frac{\partial^2 T}{\partial y^2} \tag{13}$$

The partial differential equations (3), (5) and (13) are transformed into ordinary differential equations by introducing the dimensionless variables are given by (14):

$$\psi=\sqrt{\frac{b\nu}{(1-\zeta t)}}xf(\eta),\eta=\sqrt{\frac{b}{\nu(1-\zeta t)}}y,T=T_\infty+T_0\left(\frac{bx(1-\zeta t)^{-2}}{2\nu}\right)\theta(\eta),C=C_\infty+C_0\left(\frac{bx(1-\zeta t)^{-2}}{2\nu}\right)\phi(\eta) \quad (14)$$

The stream function velocity ψ can be defined as $u=\frac{\partial\psi}{\partial y},v=-\frac{\partial\psi}{\partial x}$ so that equation (2) satisfies the continuity equation (2). $f(\eta)$ denote the injection and suction, η is the dimensionless space variable, $\theta(\eta)$ and $\phi(\eta)$ are the dimensionless of temperature and concentration of the fluid respectively.

In view of the above mentioned transformations equations (3),(5) and (13) are reduced to the following ODEs:

$$\left(1+\frac{1}{\beta}\right)f'''+ff''-(f')^2-\delta\left(0.5\eta f''+f'\right)-\left(M+\frac{1}{K}\right)f'+\lambda_1\theta+\lambda_2\phi=0 \quad (15)$$

$$\left(1+\frac{4}{3}R\right)\theta''+\Pr\left[f\theta'-f'\theta-\delta\left(0.5\eta\theta'+2\theta\right)\right]=0 \quad (16)$$

$$\phi''+Sc\left(f\phi'-f'\phi\right)-Sc\delta\left(0.5\eta\phi'+2\phi\right)-KrSc\phi=0 \quad (17)$$

With the transformed boundary conditions of the problem are:

$$f(0)=S,\ f'(0)=1+k_1f''(0),\theta(0)=1+k_2\theta'(0),\phi(0)=1+k_3\phi'(0)$$
$$f'(\infty)\to0,\theta(\infty)\to0,\phi(\infty)\to0 \quad (18)$$

The dimensionless constants δ, λ_1, λ_2, M,K, Pr,R,Sc,Sr,Kr, k_1,k_2,k_3 represent the parameters of unsteadiness parameter, buoyancy parameters, magnetic parameter, permeability parameter, Prandtl number, radiation parameter, Schmidt number, Soret number, chemical reaction rate, velocity slip parameter, thermal slip parameter and concentration slip parameter respectively.

The quantities of physical interest in this problem are the skin friction coefficient, Nusselt number and the Sherwood number can be expressed as:

$$Cf_x=\frac{\mu}{\rho u_w^2}\left(\frac{\partial u}{\partial y}\right)_{y=0},$$
$$Nu=\frac{x}{\kappa\left(T_w-T_\infty\right)}\left[\kappa\left(\frac{\partial T}{\partial y}\right)_{y=0}-\frac{4\sigma^*}{3k^*}\left(\frac{\partial T^4}{\partial y}\right)_{y=0}\right], \quad (19)$$
$$Sh=-\frac{x}{\left(C_w-C_\infty\right)}\left(\frac{\partial C}{\partial y}\right)_{y=0}$$

Substituting equation (14) into (19) to obtain the final dimensionless form:

$$Cf_r=\sqrt{\mathrm{Re}_x}\,f''(0),Nu_r=\frac{Nu}{\sqrt{\mathrm{Re}_x}}=-\theta'(0),\mathrm{Sh}_r=\frac{Sh}{\sqrt{\mathrm{Re}_x}}=-\phi'(0) \quad (20)$$

where Re_x is the local Reynolds, Cf_r is the reduced skin friction, Nu_r is the reduced Nusselt number and *Shr* is the reduced Sherwood number.

3. RESULT AND DISCUSSION

The theoretical framework examining the influence of slip effects on the unsteady magnetohydrodynamic (MHD) flow of Casson nanofluid over a porous stretching surface, incorporating thermal radiation and chemical reactions, is delineated in this research. The governing equations of the flow are represented as a system of partial differential equations, which are subsequently transformed into a set of coupled total differential equations utilizing the methodology of similarity transformation. The resulting transformed equations were subsequently resolved through the application of the Runge-Kutta Fehlberg method in conjunction with shooting techniques.

Figure 2 showcases the relationship between the magnetic parameter (M) and the velocity profile. It can be seen in Figure 2 that boosting the magnetic parameter corresponds with a lower velocity profile. The magnetic field is applied perpendicularly to the concurrent flow of the Casson fluid, thereby inducing a drag-like force, specifically the Lorentz force. This force plays a crucial role in attenuating the motion of the electrically conducting fluid. Hence, this force induces a lowering of the velocity profile, as evidenced in Figure 2. Our experimental findings demonstrate that the velocity profile, as represented in Figure 2, gradually decreases from the wall to the dimensionless distance. Given the non-uniform velocity illustrated in the momentum equation (3), the reduction in fluid motion is not uniform across the span from the initial point to the boundary, which tends toward zero. From a physical perspective, if the product of electrical conductivity and the intensity of the magnetic force exceeds the fluid density, the Lorentz force exerts a greater electromagnetic influence, consequently decelerating and impeding the fluid motion to a greater extent.

Figure 3 depicts how the Casson parameter impacts the velocity profile. When the value of this parameter goes up, the velocity profile diminishes, as evidenced by Figure 3. Our experimental findings indicate that the flow characteristics of Casson nanofluid, in conjunction with the presence of Lorentz force, contribute to the deterioration of fluid motion. Furthermore, the yield-stress exhibiting fluid is characterized by a plastic dynamic viscosity. A liquid's viscosity provides opposition to how it flows. Consequently, the plastic dynamic viscosity, which is regarded as constant throughout this investigation, represents an additional metric for the attenuation of fluid velocity. This implies that heightened plastic dynamic viscosity engenders increased resistance to the flow. The values of the Casson parameter are selected within the range of $0<\beta<2$. This values are chosen to be small because we observed that as we keep increasing the value of $\beta (i.e\ as\ \beta \longrightarrow \infty)$, the present model transformed to be only flow of Williamson nanofluid. This means that when $\beta \longrightarrow \infty$ in the viscosity term $\nu\left(1+\frac{1}{\beta}\right)\frac{\partial^2 u}{\partial y^2}$ we have $\nu\left(1+\frac{1}{\infty}\right)\frac{\partial^2 u}{\partial y^2}=\nu\frac{\partial^2 u}{\partial y^2}$. Obviously, the Casson fluid model is negligible as $\beta \to \infty$.

Figure 4 delineates the influence of the permeability parameter on the velocity distribution. The permeability parameter facilitates the mobility of Casson fluid within the boundary layers. In an optimal scenario, the aperture permits a continuous flow of Casson fluid throughout the boundary layers. The transport of fluid particles within these layers becomes significantly elevated as the parameter increases. Figure 4 presents a vivid depiction of this phenomenon, highlighting how an increase in the permeability parameter leads to enhancements in the velocity profile and a thicker momentum boundary layer. In Figures 5(a-c), the repercussions of the unsteadiness parameter are observed to enhance the velocity profile while concurrently diminishing both the temperature and concentration profiles. This occurs because, when unsteadiness is encountered within the fluid environment, the fluid particles exhibit rapid and erratic movement within the boundary layer. Such randomness effectively reduces the temperature of the fluid particles and their concentration.

The influence of the thermal buoyancy parameter on the velocity distribution is illustrated in figure 6. It is observed that the buoyancy force parameter enhances the velocity profile as its magnitude increases. Investigative results demonstrate that an elevation in this metric corresponds with a reduction in fluid viscosity, facilitating swifter fluid dynamics. Consequently, further increments in this parameter induce a significant escalation in the velocity profile, as depicted in figure 6. The mass buoyancy force parameter is similarly observed to augment the velocity profile with increasing values, as demonstrated in figure 7. Real-world observations support the idea that a greater mass buoyancy metric correlates with a decrease in fluid viscosity,

resulting in more rapid fluid movement. Therefore, elevated values of mass buoyancy correlate with an enhancement in the velocity profile, as illustrated in figure 7.

Figure 8 illustrates the effect of Prandtl number (Pr) on temperature profile. $\mathrm{Pr} = \frac{\rho c_p}{k^*}$ is noticed to decrease the temperature profile. It worth noting that thermal diffusivity $\alpha = \frac{1}{\rho c_p}$, hence Pr is the inverse of thermal diffusivity. Pr is noticed to degenerate the temperature profile gradually from the wall. This is because there is not much viscosity far away from the plate. Greater Pr is very useful in controlling thermal diffusivity as well as momentum diffusivity in heat along with mass transport problem. Note that $\mathrm{Pr} = 0.72, 1.0, 3.0, 7.0$ used in this study implies Pr for water. Hence, when $\mathrm{Pr} << 1$ it implies thermal diffusivity controls the flow behavior while $\mathrm{Pr} >> 1$ implies momentum diffusivity controls the flow behavior. Therefore, Pr is useful in controlling cooling rate of an electrically conducting fluid. In this study, there exist a wall temperature T_w and free stream temperature T_∞ which gives rise to $(T_w - T_\infty)$ along with thermal boundary layer thickness. Figure 9 depicts the effect of thermal radiation (R) on the temperature profile. The thermal radiation makes thermal condition of the fluid to enhance. The use of Roseland approximation in approximating the radiative heat flux in the present study warms up the fluid within the thermal boundary layer. Now, increase in R boast the temperature along with the thermal boundary layer thickness as illustrated in figure 9.

Figure 10 illustrates the influence of Schmidt number (Sc) on the concentration distribution. It can be discerned from figure 10 that an elevation in the value of deteriorates the concentration distribution. The inverse relationship of the Brownian diffusion coefficient is . Thus, as the moment is augmented, it diminishes the Brownian diffusion, which consequently results in a reduction of solutal concentration. Our numerical simulations indicate that an increase in results in a concomitant diffusion of species at a uniform rate. It is noteworthy that when , there exists a significant diffusion of species surpassing the momentum diffusivity. Clearly, establishing implies the non-existence of species concentration. Presently, an increase in diminishes the fluid concentration and subsequently lowers its distribution profile.

Figure 11 elucidates the influence of the Soret number on the concentration distribution. An elevated value of the Soret number is observed to enhance the concentration distribution. The Soret term constitutes a second-order function incorporated into the concentration equation. The inclusion of this term within the concentration equation is anticipated to modify the concentration profile within the boundary layer. Furthermore, a thermal diffusion of fluid particles is observed transitioning from regions of lower concentration to regions of higher concentration as the Soret number increases.

Figure 12 illustrates the impact of the chemical reaction parameter on the concentration distribution. An increase in this parameter is associated with a reduction in the solutal concentration profile, indicating a potentially destructive reaction. An escalation in the chemical reaction rate poses a significant risk to the flow of blood, thereby endangering animal health. The observed decline in the concentration profile due to an increase in the chemical reaction parameter may be attributed to the influence of the externally applied magnetic field aligned with the flow direction. The ramifications of suction velocity on the velocity profile are depicted in Figure 13. A heightened suction velocity is found to diminish the velocity profile. This observation suggests that an increased suction velocity corresponds to augmented viscosity, consequently impeding the motion of fluid particles within the boundary layer. The implications of the slip parameters are delineated in Figures 14(a-c). It is discerned that the slip parameters contribute to the reduction of the hydrodynamic, thermal, and concentration boundary layer thickness. Consequently, the profiles of velocity, temperature, and concentration exhibit an overall decrease throughout the boundary layer.

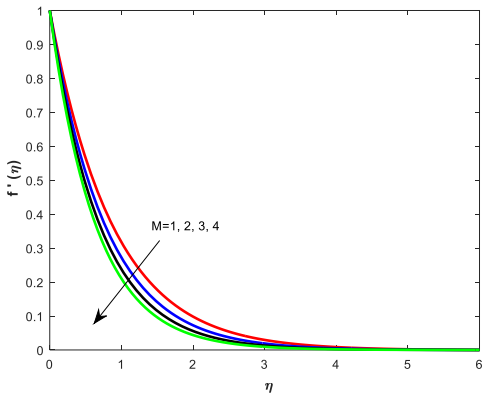

Fig.2. Velocity profiles for different values of magnetic parameter (M).

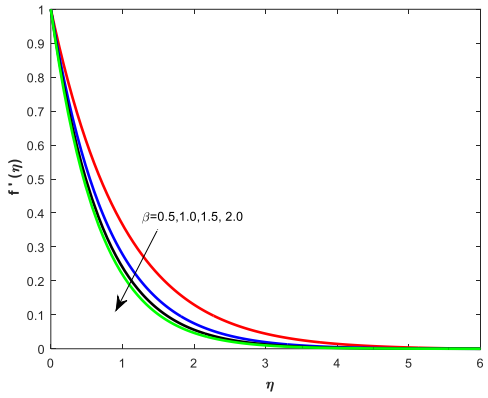

Figure 3: Effect of Casson parameter on the velocity profile (β)

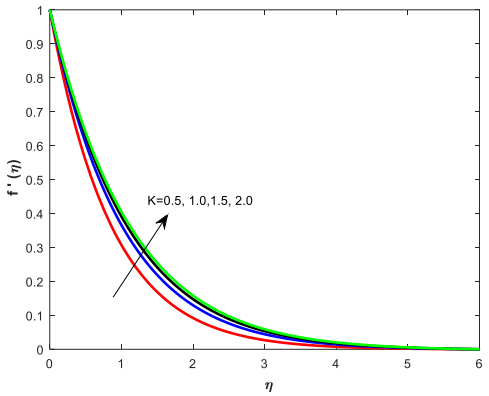

Figure 4: Effect of the permeability parameter on the velocity profile (K).

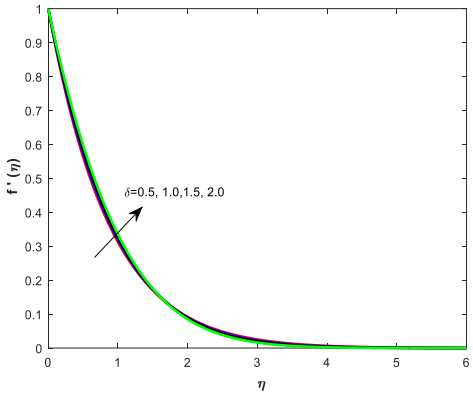

Figure 5(a): Effect of unsteadiness parameter (δ) on the velocity profiles.

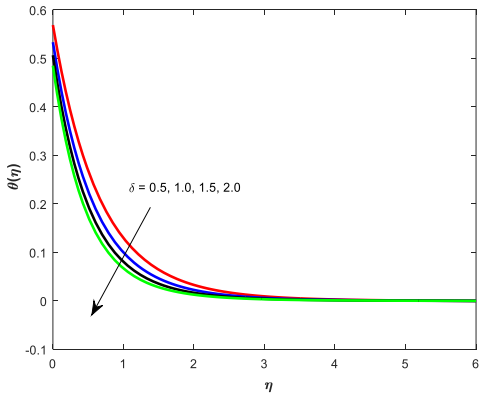

Figure 5(b): Effect of unsteadiness parameter (δ) on the temperature profiles.

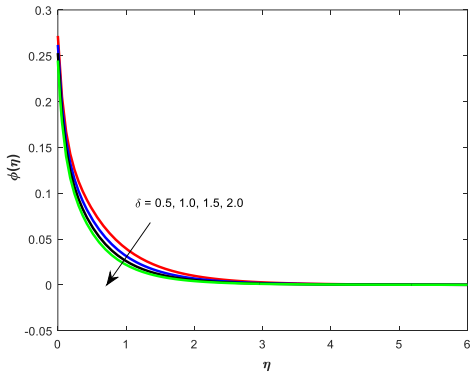

Figure 5(c): Effect of unsteadiness parameter (δ) on the concentration profiles.

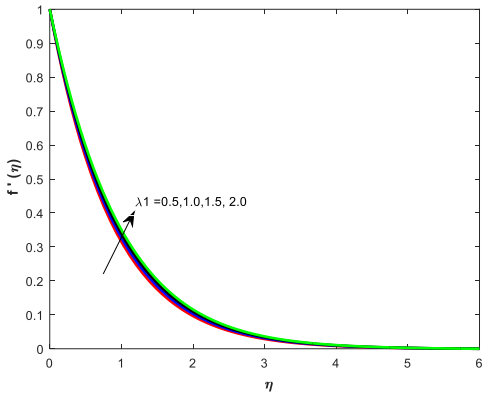

Figure 6: Effect of thermal buoyancy on the velocity profile.

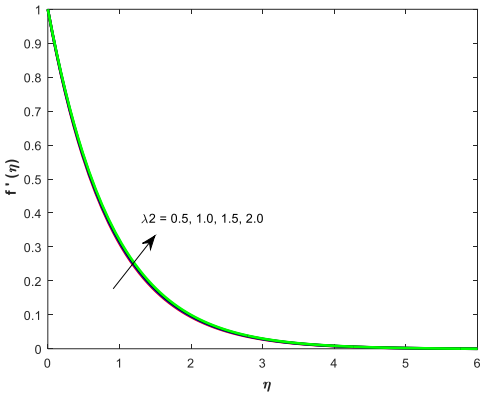

Figure 7: Effect of mass buoyancy parameter on the velocity profile.

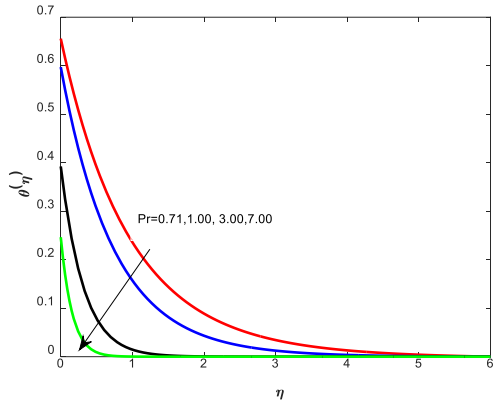

Figure 8: Effect of Prandtl number on the temperature profile.

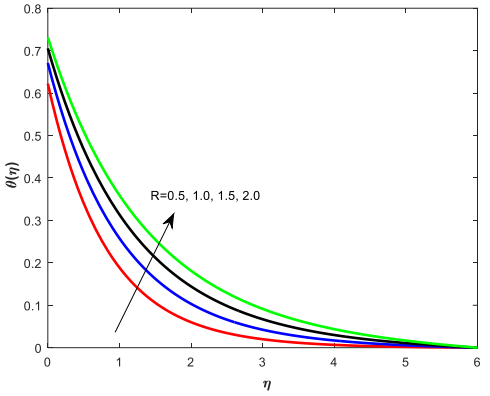

Figure 9: Effect of thermal radiation parameter on the temperature profile.

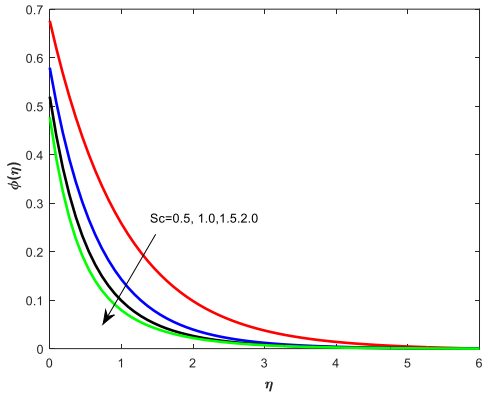

Figure 10: Effect of the Schmidt number on the concentration profile.

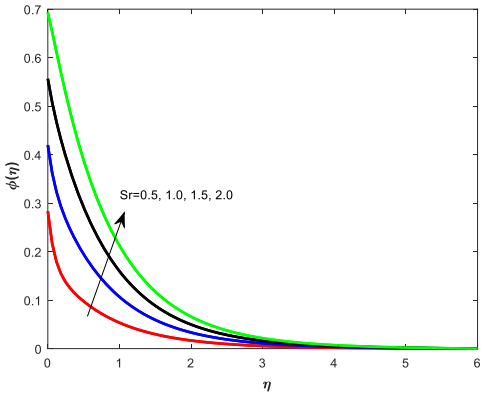

Figure 11: Effect of Soret number on the concentration profile.

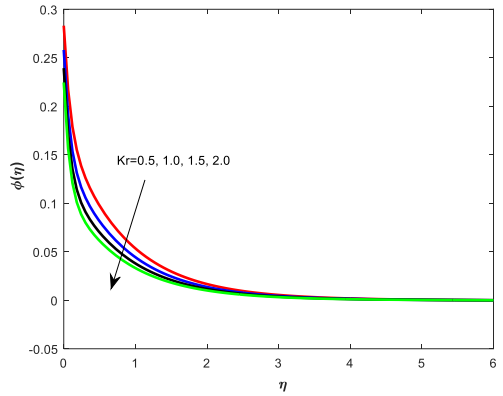

Figure 12: Effect of chemical reaction parameter on the concentration profile.

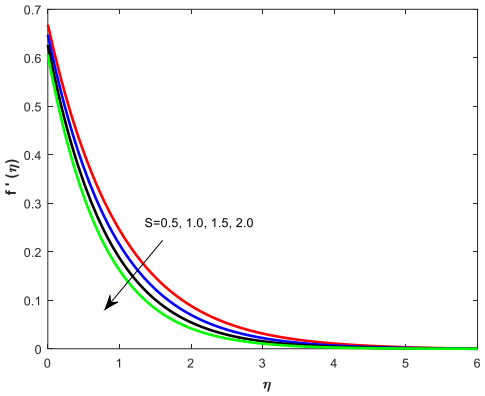

Figure 13: Effect of suction velocity on the velocity profile.

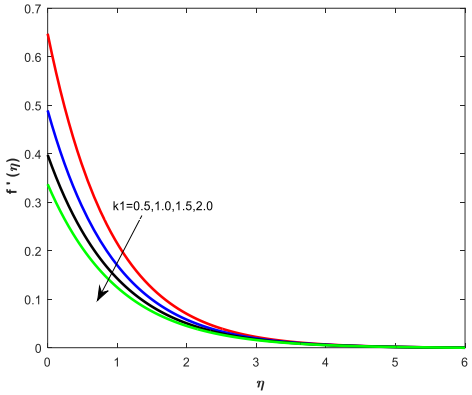

Figure 14 (a): Effect of the velocity slip parameters.

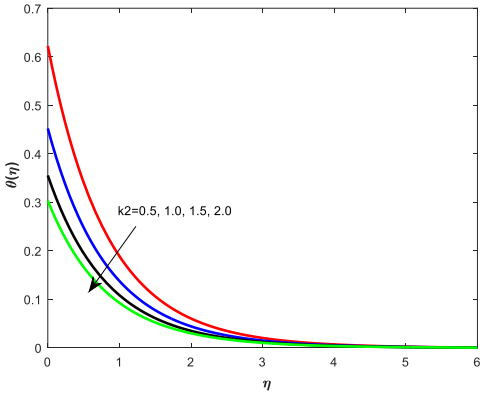

Figure 14 (b): Effect of the thermal slip parameters.

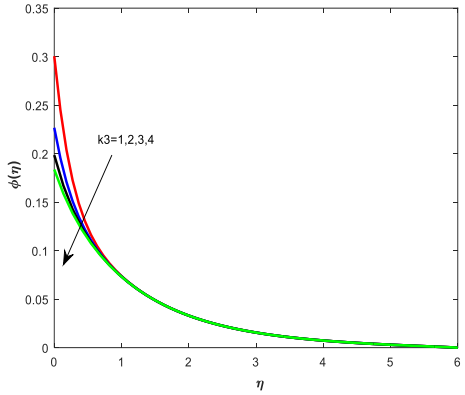

Figure 14(c): Effect of the concentration slip parameters.

Table 1 shows the computational values for pertinent flow parameters on skin friction coefficient, Nusselt and Sherwood number. Controlling parameters are observed to elevate the skin friction coefficient, Nusselt and Sherwood number.

Table 1: Effect of pertinent flow parameters on the skin friction coefficient, Nusselt and Sherwood number.

M	B	K	d	L1	L2	Pr	R	Sc	Sr	Kr	S	k1	k2	k3	Cf	Nu	Sh
1	0.5	1	0.2	0.2	0.2	1	0.5	10	0.5	0.5	1	0	0.5	0.5	1.133341	0.788478	1.442514
2															1.289988	0.793748	1.443095

3															1.427898	0.799862	1.443804
4															1.552470	0.807156	1.444703
0.2	0.5	1	0.2	0.2	0.2	1	0.5	10	0.5	0.5	1	0	0.5	0.5	0.987949	0.790242	1.442714
	1														1.259360	0.794315	1.443168
	1.5														1.408560	0.801016	1.443950
	2														1.504014	0.814239	1.445635
0.2	0.5	0.5	0.2	0.2	0.2	1	0.5	10	0.5	0.5	1	0.5	0.5	0.5	0.883487	0.805579	1.444504
		1													0.919764	0.814239	1.445635
		1.5													0.987949	0.817652	1.446106
		2													1.166554	0.819489	1.446365
0.2	0.5	0.5	0.5	0.2	0.2	1	0.5	10	0.5	0.5	1	0.5	0.5	0.5	0.964000	0.862220	1.456677
			1												1.022661	0.933052	1.476423
			1.5												1.079727	0.986748	1.494315
			2												1.134790	1.029991	1.510292
0.2	0.5	0.5	0.2	0.5	0.2	1	0.5	10	0.5	0.5	1	0.5	0.5	0.5	1.007749	0.806785	1.444658
				1											1.051112	0.808732	1.444913
				1.5											1.095031	0.810607	1.445165
				2											1.139543	0.812416	1.445413
0.2	0.5	0.5	0.2	0.2	0.5	1	0.5	10	0.5	0.5	1	0.5	0.5	0.5	1.114006	0.805946	1.444551
					1										1.128551	0.806553	1.444630
					1.5										1.143135	0.807153	1.444708
					2										1.157760	0.807747	1.444786
0.2	0.5	0.5	0.2	0.2	0.2	0.71	0.5	10	0.5	0.5	1	0.5	0.5	0.5	1.161833	0.688246	0.895098
						1									1.166554	0.805579	1.161202
						3									1.177277	1.215335	1.444504
						7									1.181596	1.507259	1.507911
0.2	0.5	0.5	0.2	0.2	0.2	0.71	0.5	10	0.5	0.5	1	0.5	0.5	0.5	0.698743	0.536958	1.433801
							1								0.700465	0.589052	1.490504
							1.5								0.702559	0.658277	1.527764
							2								0.705143	0.755472	1.554127
0.2	0.5	0.5	0.2	0.2	0.2	0.71	0.5	0.5	0.5	0.5	1	0.5	0.5	0.5	0.693377	0.755962	0.647962
								1							0.698403	0.756186	0.841298
								1.5							0.700636	0.756617	0.960830
								2							0.701892	0.757711	1.045386
0.2	0.5	0.5	0.2	0.2	0.2	0.71	0.5	0.5	0.5	0.5	1	0.5	0.5	0.5	0.694662	0.755472	0.613862
									1						0.698146	0.756099	0.887141
									1.5						0.701640	0.756722	1.160454
									2						0.705143	0.757340	1.433801
0.2	0.5	0.5	0.2	0.2	0.2	0.71	0.5	0.5	0.5	0.5	1	0.5	0.5	0.5	0.705143	0.755229	1.433801
										1					0.705744	0.755287	1.483892
										1.5					0.706177	0.755364	1.521409
										2					0.706505	0.755472	1.550888
0.2	0.5	0.5	0.2	0.2	0.2	0.71	0.5	0.5	0.5	0.5	0.5	0.5	0.5	0.5	0.663426	0.666232	1.339020

											1				0.705143	0.755472	1.433801
											1.5				0.746967	0.842582	1.493874
											2				0.788485	0.924246	1.538509
0.2	0.5	0.5	0.2	0.2	0.2	0.71	0.5	0.5	0.5	0.5	0.5	0.5	0.5	0.5	0.331464	0.701736	1.425768
												1			0.401688	0.713070	1.427141
												0.5			0.510747	0.729433	1.429433
												2			0.705143	0.755472	1.433801
0.2	0.5	0.5	0.2	0.2	0.2	0.71	0.5	0.5	0.5	0.5	0.5	0.5	0.5	0.5	0.705143	0.366796	1.433801
													1		0.709612	0.429946	1.508623
													1.5		0.712167	0.547923	1.551229
													2		0.713538	0.755472	1.574058
0.2	0.5	0.5	0.2	0.2	0.2	0.71	0.5	0.5	0.5	0.5	0.5	0.5	0.5	0.5	0.622881	0.579801	0.204084
														1	0.623448	0.579818	0.267154
														0.5	0.623665	0.579851	0.386645
														2	0.623779	0.579938	0.699533

References:

[1] Mahanthesh B., Mabood F., Gireesha B. J., and Gorla R. S. R., "Effects of chemical reaction and partial slip on the three dimensional flow of a nanofluid impinging on an exponentially stretching surface," *European Physical Journal Plus*, vol. 132, no. 3, 2017.

[2] Chamkha A. J., Aly A. M., and Mansour M. A., "Similarity solution for unsteady heat and mass transfer from a stretching surface embedded in a porous medium with suction/injection and chemical reaction effects," *Chemical Engineering Communications*, vol. 197, no. 6, pp. 846–858, 2010.

[3] T. Hayat, S. Hina, and N. Ali, "Simultaneous effects of slip and heat transfer on the peristaltic flow," *Communications in Nonlinear Science and Numerical Simulation*, vol. 15, no. 6, pp. 1526–1537, 2010.

[4] S. S. Motsa and S. Shateyi, "Successive linearization analysis of the effects of partial slip, thermal diffusion, and diffusion thermo on steady MHD convective flow due to a rotating disk," *Mathematical Problems in Engineering*, vol. 2012, Article ID 397637, 15 pages, 2012.

[5] S. Shateyi and F. Mabood, "MHD mixed convection slip flow near a stagnation-point on a non-linearly vertical stretching sheet in the presence of viscous dissipation," *thermal Science*, vol. 21, no. 6, pp. 2731–2745, 2017.

[6] B. C. Prasannakumara, M. R. Krishnamurthy, B. J. Gireesha, and R. S. R. Gorla, "Effect of multiple slips and thermal radiation on MHD flow of jeffery nanofluid with heat transfer," *Journal of Nanofluids*, vol. 5, no. 1, pp. 82–93, 2016.

[7] F. Mabood, A. Shafiq, T. Hayat, and S. Abelman, "Radiation effects on stagnation point flow with melting heat transfer and second order slip," *Results in Physics*, vol. 7, pp. 31–42, 2017.

[8] Mabood, F. Multiple slip effects on MHD unsteady flow heat and mass transfer impinging on permeable stretching sheet with radiation. Model. Simul. Eng. 2019, 2019, 3052790.

[9] Sharidan, S., Mahmood, T., and Pop, I. (2006). Similarity solutions for the unsteady boundary layer flow and heat transfer due to a stretching sheet, Int. J. Appl. Mech. Eng., 11,647–654.

[10] Elbashbeshy E.M.A. and Bazid M.A.A. (2004): Heat transfer over an unsteady stretching surface. – Heat Mass Transfer, vol.41, pp.1-4.

[11] Grubka L.J. and Bobba K.M. (1985): Heat transfer characteristic of a continuous stretching surface with variable temperature. – J. Heat Transfer, vol.107, pp.248-250.

[12] Magyari E. and Keller B. (1999): Heat and mass transfer in the boundary layers on an exponentially stretching continuous surface. – J. Phys. D: Appl. Phys., vol.32, pp.577-585.

[13] Nazar R, Amin N., Filip D. and Pop I. (2004): Unsteady boundary layer flow in the region of the stagnation point on the stretching sheet. – Int. J. Eng. Sci., vol.42, pp.1241-1253.

[14] Magyari E. and Keller B. (2000): Exact solutions for self-similar boundary-layer flows induced by permeable stretching surfaces. – Eur. J. Mech. B-Fluids, vol.19, pp.109-122.
[15] Ibrahim S.M., Mabood F., Suneetha K., Lorenzini G. (2017), 'Effects of chemical reaction on combined heat and mass transfer by laminar mixed convection flow from vertical surface with induced magnetic field and radiation', Journal of Engineering Thermophysics, 26(2), PP.234-255.
[16] N Vijaya, Y Hari Krishna, K Kalyani, GVR Reddy ,Soret And Radiation Effects On An Unsteady Flow Of A Casson Fluid Through Porous Vertical Channel With Expansion And Contraction, - Frontiers in Heat and Mass Transfer (FHMT)11,2018,1-11.
[17] Reddy G.V.R., Krishna Y.H.(2018), 'Soret and dufour effects on MHD micropolar fluid flow over a linearly stretching sheet, through a non-darcy porous medium', International Journal of Applied Mechanics and Engineering ,23(2), PP. 485-502
[18] Arundhati V., Chandra Sekhar K.V., Prasada Rao D.R.V., Sreedevi G.(2018), 'Non-Darcy convective heat and mass transfer flow through a porous medium in vertical channel with soret, dufour and chemical reaction effects', JP Journal of Heat and Mass Transfer ,15(2), PP. 213-240
[19] Suneetha K., Ibrahim S.M., Reddy G.V.R.(2018), 'Radiation and heat source effects on MHD flow over a permeable stretching sheet through porous stratum with chemical reaction', Multidiscipline Modeling in Materials and Structures ,14(5), PP. 1101-1114
[20] N.Vijaya, M.Radha Madhavi &Y.Hari Krishna; "Boundary Layer Flow Of A Mixed Convective Nanofluid Over A Vertical Circular Cylinder Under The Influence Of Magnetic Field", Heat Radiation And External Surface Temperature, International Journal of Mechanical and Production Engineering Research and Development , 8(2), 411-420,2018
[21] Krishna Y.H., Reddy G.V.R., Makinde O.D.(2018), 'Chemical reaction effect on MHD flow of casson fluid with porous stretching sheet', Defect and Diffusion Forum ,389, PP. 100-109
[22] Satish Kumar D., Ramana Murthy C.H.V., Anusha S., Makinde O.D. (2019), 'Mixed convective flow of a visco elastic fluid between two porous parellel plates', International Journal of Recent Technology and Engineering, 8(3), PP.4830-4834.
[23] Manjula V., Chandra Sekhar K.V. (2019), 'Effect of Soret number and heat source on unsteady MHD Casson fluid flow past an inclined plate embedded in porous medium', ARPN Journal of Engineering and Applied Sciences, 14(11), PP.2069-2079.
[24] Vijaya K., Reddy G.V.R. (2019), 'Magnetohydrodynamic casson fluid flow over a vertical porous plate in the presence of radiation, soret and chemical reaction effects', Journal of Nanofluids, 8(6), PP.1240-1248.
[25] Sujatha T., Jayarami Reddy K., Kumar J.G. (2019), 'Chemical reaction effect on nonlinear radiative MHD nanofluid flow over cone and wedge', Defect and Diffusion Forum, 393, PP.83-102.
[26] Kallepalli N.S., Rajasekhar K., Ramana Murthy C.V. (2019), 'Influence of critical parameters on an unsteady state mhd flow in a porous channel with exponentially decreasing suction', Journal of Mathematical and Computational Science, 9(6), PP.764-783.
[27] Sivaiah G., Jayarami Reddy K., Chandra Reddy P., Raju M.C. (2019), 'Numerical study of mhd boundary layer flow of a viscoelastic and dissipative fluid past a porous plate in the presence of thermal radiation', International Journal of Fluid Mechanics Research, 46(1), PP.27-38.
[28] Aruna, Ganjikunta., R., Koka. (2024). 1. Study of MHD Casson Nanofluid Flow Over an Inclined Stretching Sheet in Porous Media with Thermal Slip, Chemical Reaction and Radiation Effects. CFD Letters, doi: 10.37934/cfdl.17.3.167195
[29] Arick, M., Lakhani. (2024). 2. Heat and Mass Transfer in MHD Flow of a Nanofluid through a Porous Medium over a Stretching Sheet with Chemical Reaction. Deleted Journal, doi: 10.52783/cana.v31.1518.
[30] M, Hema, Radhika., Y., Dharmendar, Reddy. (2024). 4. Influence of velocity and thermal slips on Magneto Casson fluid heat transmission flow past an exponential porous stretching surface with chemical reaction and radiation. Modern Physics Letters B, doi: 10.1142/s0217984925500241